Accurate Calculation of Zero-Field Splittings of (Bio)inorganic Complexes: Application to an $\{FeNO\}^7$ (S = 3/2) Compound

Fredy Aquino and Jorge H. Rodriguez*

Theoretical and Computational Biomolecular Physics Group, Department of Physics, Purdue University, West Lafayette, Indiana 47907-2036

Received: December 8, 2008; Revised Manuscript Received: July 1, 2009

Iron nitrosyl complexes with $\{FeNO\}^7$ (S = 3/2) configuration have a complex electronic structure and display remarkable but not fully understood spectroscopic properties. In particular, $\{FeNO\}^7$ (S = 3/2) complexes have very large zero-field splittings (ZFSs), which arise from strong spin−orbit coupling, a relativistic effect. The accurate prediction and microscopic interpretation of ZFSs in transition metal complexes can aid in the interpretation of a vast amount of spectroscopic (e.g., Mössbauer and electron paramagnetic resonance) and other experimental (e.g., magnetic susceptibility) data. We report the accurate calculation of the sign and magnitude of ZFSs for a set of representative diatomic molecules based on a combined spin density functional theory and perturbation theory (SDFT-PT) methodology. In addition, we apply the SDFT-PT methodology to accurately calculate the magnitude and sign of the ZFS parameters of an $\{FeNO\}^7$ (S = 3/2) complex and to interpret its spectrocopic data. We find that the principal component D_{zz} of the ZFS tensor is very closely oriented along the Fe−N(O) bond, indicating that nitric oxide dominates the very intricate electronic structure of the $\{FeNO\}^7$ (S = 3/2) compound. We find a direct correlation between electronic delocalization along the Fe−N(O) bond, which is due to π-bonding, and the large ZFS.

1. Introduction

The geometric structures, bonding properties, and chemical reactivities of transition metal nitrosyls have been important subjects of study.[1,2] In particular, the study of iron nitrosyls with a $\{FeNO\}^7$ configuration[1−3] and intermediate spin (S = 3/2) ground state is of great theoretical and chemical importance. At the theoretical level, $\{FeNO\}^7$ (S = 3/2) complexes possess a complicated valence electronic structure[4−11] that gives rise to intriguing spectroscopic parameters. For example, $\{FeNO\}^7$ (S = 3/2) complexes exhibit Mössbauer isomer shifts ($\delta_{Fe} \approx 0.62-0.66$ mm/s),[11−14] which are intermediate between those of typical high-spin ferric and high-spin ferrous configurations,[11] and also unusual electron paramagnetic resonance (EPR) signals.[14−16] In addition, $\{FeNO\}^7$ (S = 3/2) complexes display unusually large zero-field splitting (ZFS) parameters ($D \approx 12-20$ cm^{-1}),[10−13] which remove the degeneracy of their quartet spin ground states as illustrated by Figure 1. Intermediate spin $\{FeNO\}^7$ complexes are also important because these mimic many spectroscopic and some structural properties of mononuclear[12,13] and binuclear[11,16] iron centers in proteins that are known to bind nitric oxide.

Despite its importance, little theoretical work has been done to predict and explain, in terms of electronic structure calculations, the intriguingly large ZFS parameters of $\{FeNO\}^7$ (S = 3/2) complexes. One main reason is that ZFSs of transition metal complexes are intimately related to the action of spin−orbit coupling (SOC),[17] an interaction that is not incorporated in conventional (nonrelativistic) Hartree−Fock or Kohn−Sham (KS) density functional theory calculations.[18−20]

ZFSs are central to the analysis of a vast amount of experimental data. In particular, spectra from Mössbauer and EPR experiments as well as magnetic susceptibility of bioinorganic complexes and metalloproteins are often interpreted in terms of spin Hamiltonians, which include a ZFS interaction.[10−13,21,22] Therefore, the development and implementation of methods of electronic structure capable of predicting and interpreting ZFS of metal complexes has the potential to explain, at the microscopic level, a large body of spectroscopic and other experimental data.

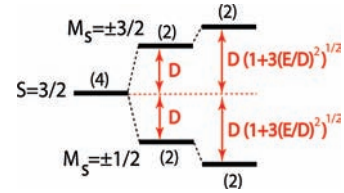

Figure 1. Effect of axial (D) and rhombic (E) ZFS parameters on energy levels of S = 3/2 systems. The notation used is defined by eqs 1 and 2.

Until recently, the accurate prediction and microscopic interpretation of ZFSs of bioinorganic complexes had remained a formidable challenge. One major development that paved the way for the computation of ZFS parameters has been the pioneering work of Pederson et al.[23,24] that treats SOC effects within the framework of perturbation theory (PT). These authors have mainly focused on the computation of the closely related concept of magnetic anisotropies in molecular magnets.[23,24] At the same time, although some wave function-based ab initio approaches exist for the accurate computation of SOC effects in small organic molecules,[25] these are computationally expensive and generally impractical for large transition metal-containing complexes. Therefore, there was need to implement accurate methods for the computation of ZFSs of bioinorganic complexes.

In addition to its relevance to bioinorganic magnetism, it is highly desirable to computationally predict ZFSs as an aid in

* To whom correspondence should be addressed. E-mail: jorge-r@physics.purdue.edu.

10.1021/jp8107667 CCC: $40.75
Published on Web 07/22/2009

the design of metal-containing single-molecule magnets, in particular, in the design of clusters that have an intrinsically large and negative ZFS, since these are possible building blocks for highly dense memory storage devices.[26−28]

Recently, we reported the implementation of a method that accurately predicts the ZFS of complexes of uniaxial symmetry at a moderate computational cost.[29] More specifically, we reported the implementation of a combined spin density functional theory (SDFT) and PT methodology (SDFT-PT), which incorporates the effects of SOC via PT on top of a nonrelativistic SDFT calculation.[29] In this work, we briefly describe the generalization of this method for complexes of lower (arbitrary) symmetry. In addition, we focus on the prediction and interpretation of the unusually large ZFS parameters of an $\{FeNO\}^7$ (S = 3/2) complex. Consistent with our previous results,[29] we show that our SDFT-PT method is capable of computing ZFS parameters with good accuracy. We also show that our SDFT-PT calculations provide a much needed correlation between molecular structure, electronic structure, and ZFS parameters obtained from experiment.

2. Theoretical and Computational Methods

Although nonrelativistic KS-SDFT[18−20] is an efficient method for elucidating ground state electronic structures of metal complexes, it does not incorporate SOC. Therefore, by themselves, KS-SDFT calculations cannot compute ZFSs, which are intimately related to the action of SOC, a relativistic effect. For many cases of interest, however, SOC can be considered a perturbation to the electronic Hamiltonian of a molecular system. Consequently, some authors have derived expressions that use nonrelativistic KS-SDFT in conjunction with sum-overstates PT to incorporate the effects of SOC.[23,30] On the basis of these studies, we previously implemented expressions for computing ZFS parameters of complexes of uniaxial symmetry.[29] We have now implemented expressions for computing ZFS parameters of complexes of arbitrary symmetry.

In some organic complexes, there is a sizable contribution from spin−spin (SS) interactions to their ZFS. In transition metal complexes, however, the SOC contribution to the ZFS is normally dominant.[31] As reviewed by Kahn,[17] ZFSs of metal complexes result from the combined action of ligand fields and SOC. The ligand fields acting on valence electrons are included in nonrelativistic SDFT via the electron−nuclear interactions. Therefore, to compute ZFS parameters, one can incorporate the effects of SOC by means of PT on top of a KS-SDFT calculation. To accomplish this, however, one needs to establish a relationship between solutions to the one-electron KS electronic Hamiltonians and the phenomenological ZFS parameters. In what follows, we outline such relationship and present explicit expressions for the ZFS parameters.

The phenomenological ZFS Hamiltonian is written in terms of the operator $\mathbf{S}$ corresponding to the spin ground state of a particular complex and the ZFS tensor $\tilde{D}$:[11,17,21,22]

$$\mathscr{H}_{ZFS} = \mathbf{S}\cdot\tilde{\mathrm{D}}\cdot\mathbf{S} \tag{1}$$

The tensor $\tilde{D}$ is chosen to be traceless, and the ZFS interaction can be expressed in terms of axial (D) and rhombic (E) parameters:

$$\mathscr{H}_{ZFS} = \mathrm{D}\left[S_z^2 - \frac{1}{3}S(S+1)\right] + \mathrm{E}(S_x^2 - S_y^2) \tag{2}$$

$$\mathrm{D} = \frac{3}{2}\mathrm{D}_{zz} \tag{3}$$

$$\mathrm{E} = \frac{1}{2}(\mathrm{D}_{xx} - \mathrm{D}_{yy}) \tag{4}$$

where D_{xx}, D_{yy}, and D_{zz} are the diagonal components of the ZFS tensor ($\tilde{D}$) in its principal axes *xx*, *yy*, and *zz*, respectively. For complexes with uniaxial anisotropy, the rhombic term vanishes. More generally, however, E can be finite. Figure 1 illustrates the effect of ZFS parameters on the spin states of a complex with S = 3/2 ground state.

The initial stage of the SDFT-PT calculations is based on obtaining KS orbitals, $\phi_i(\mathbf{r})$, for the ground state. KS theory[18−20] yields the ground state electronic density, $\rho(\mathbf{r})$, and energy of a many-electron system from self-consistent solutions of one-electron eigenvalue equations

$$\mathscr{H}^{KS}\phi_i(\mathbf{r}) = \epsilon_i\phi_i(\mathbf{r}) \tag{5}$$

where $\rho(\mathbf{r}) = \Sigma_{i=1}^{occ}|\phi_i(\mathbf{r})|^2$. To allow for spin polarization, one can apply a spin unrestricted (U) formalism, which allows α and β electrons to occupy orbitals with different energy and spatial localization.[19,32−34]

One can derive expressions for the computation of ZFS parameters[29] by doing sum-overstates PT over the space of the KS orbitals.[23,24,30] Accordingly, the SOC operator can be written as

$$h_{SOC}(1) = \frac{1}{2c^2}\mathbf{S}\cdot\mathbf{p}\times\nabla\Phi(\mathbf{r}) \tag{6}$$

where the Coulomb potential is given by $\Phi(\mathbf{r}) = -\Sigma_n(Z_n/|\mathbf{r} - \mathbf{R}_n|) + \int d^3\mathbf{r}'[\rho(\mathbf{r}')/|\mathbf{r} - \mathbf{r}'|]$ and the electron density is related to the KS orbitals as mentioned above. Using second-order PT, one can estimate the contribution from $h_{SOC}(1)$ to the total electronic energy (in a.u.) as

$$\Delta = \sum_{\sigma\sigma'}\sum_{pq} M_{pq}^{\sigma\sigma'}S_p^{\sigma\sigma'}S_q^{\sigma'\sigma} \tag{7}$$

$$M_{pq}^{\sigma\sigma'} = M_{qp}^{\sigma\sigma'*} \equiv \sum_{ij}\frac{\langle\phi_{i\sigma}|V_p|\phi_{j\sigma'}\rangle\langle\phi_{j\sigma'}|V_q|\phi_{i\sigma}\rangle}{\epsilon_{i\sigma} - \epsilon_{j\sigma'} + \int\frac{\partial v_{xc}[\rho]}{\partial\rho}\rho_i\rho_j\,d\mathbf{r}} \tag{8}$$

$$S_p^{\sigma\sigma'} \equiv \langle\chi_\sigma|S_p|\chi_{\sigma'}\rangle \tag{9}$$

The integral term in the denominator of eq 8 is a correction to the energy difference between occupied and empty orbital energies ($\epsilon_{i\sigma} - \epsilon_{j\sigma'}$) and is dependent on the particular exchange-correlation functional with $\rho_i \equiv \phi_i^*\phi_i$.[30,35] Our initial estimates based on calculations for diatomic molecules indicate that $\int(\partial v_{xc}[\rho]/\partial\rho)\rho_i\rho_j\,d\mathbf{r}$ changes the numerical values of D by a relatively small fraction. More specifically, upon inclusion of this latter term with the BLYP and BPW91 functionals, D increased $\approx 7.7\%$ for the diatomic S_2.[36] This correction is likely of comparable magnitude for metal complexes and was not included in the present calculations on the iron nitrosyl complex.

TABLE 1: Table of Experimental and Theoretical ZFS Parameters for Selected Diatomics

	internuclear distance (a.u.)[a]	$D_{SOC+SS}^{experiment}$ (cm^{-1})[b]	$D_{SOC+SS}^{SCF-CI25}$ (cm^{-1})	$D_{SOC}^{SCF-CI25}$ (cm^{-1})	$D_{SOC}^{SDFT-PT}$ (cm^{-1})[c]
O_2	2.300	+3.96[38]	+3.972	+2.480	+3.14
PH	2.708	+4.420[39]	+3.824	+3.492	+4.61
PF	3.005	+5.92[40]	+5.410	+4.926	+6.80
SO	2.799	+10.540[41]	+10.698	+10.142	+9.90
S_2	3.567	+23.54[42]	+20.594	+20.330	+21.69

[a] To allow for direct comparison with SCF-CI results, bond lenghts used in ref 25 were also used in SDFT-PT calculations. [b] Some D values were obtained from fits to experimental data with no reported uncertainty. Numerical values are shown after conversion to present notation according to eq 2. [c] SDFT calculations done for triplet states of neutral molecules at the UBLYP/6-311G* level.

In eqs 8 and 9, $V_p \equiv (-i/2c^2)[\nabla \times \nabla\Phi(\mathbf{r})]_p$, where p,q = x,y,z, $\phi_{i\sigma}$ and $\phi_{j\sigma'}$ represent occupied and unoccupied KS orbitals, respectively, χ are generalized spinor functions,[23] and σ, σ' represent up or down spin. The matrix elements $\langle\phi_{i\sigma}|V_p|\phi_{\sigma'}\rangle$ are given by

$$\langle\phi_{i\sigma}|V_p|\phi_{j\sigma}\rangle = \frac{-i}{2c^2}\left(\left\langle\frac{d\phi_{i\sigma}}{dq}\middle|\Phi\middle|\frac{d\phi_{j\sigma'}}{ds}\right\rangle - \left\langle\frac{d\phi_{i\sigma}}{ds}\middle|\Phi\middle|\frac{d\phi_{j\sigma'}}{dq}\right\rangle\right) \tag{10}$$

where p,q,s = (x,y,z), (y,z,x), or (z,x,y). We compute $\langle(d\phi_{i\sigma}/dq)|\Phi|(d\phi_{j\sigma'}/ds)\rangle$ by expanding the KS orbitals $\phi_{i\sigma}$ in terms of Cartesian Gaussian type orbitals (CGTO). For the case where $M_{pq}^{\sigma\sigma'} = 0$ and $p \neq q$, we have derived the following expressions for the SOC contributions to the axial (D)[29] and rhombic (E) ZFS parameters with respect to the principal axes of a molecular system

$$D = \left(\frac{1}{\Delta N}\right)^2[M_{zz}^{11} + M_{zz}^{22} - M_{zz}^{12} - M_{zz}^{21} + \frac{1}{2}(M_{xx}^{12} + M_{xx}^{21} + M_{yy}^{12} + M_{yy}^{21}) - \frac{1}{2}(M_{xx}^{11} + M_{xx}^{22} + M_{yy}^{11} + M_{yy}^{22})] \tag{11}$$

$$E = \left(\frac{1}{\Delta N}\right)^2\frac{1}{2}[M_{xx}^{11} + M_{xx}^{22} + M_{yy}^{12} + M_{yy}^{21} - (M_{yy}^{11} + M_{yy}^{22} + M_{xx}^{12} + M_{xx}^{21})] \tag{12}$$

where ΔN is the difference between the number of electrons with up and down spin in the ground state. Equations 11 and 12 are of crucial importance because these relate the phenomenological ZFS parameters (D, E) to the KS orbitals, $\phi_i(\mathbf{r})$, and their corresponding eigenvalues ϵ_i.

The sum-overstates PT calculations were done with a locally developed algorithm.[29] The set of KS orbitals needed for the SDFT-PT calculations was generated from spin unrestricted (U) calculations carried out with Gaussian 98[37] on the crystallographic structure.

3. Results and Discussion

3.1. Validation of SDFT-PT Algorithm for Diatomic Molecules. Table 1 shows experimental and predicted ZFSs for some diatomic molecules. The third and fourth columns show the combined contributions from SOC and SS interactions as obtained by previous authors from fits to experiment and high level (SCF-CI) ab initio calculations, respectively.[25] Most of the latter values, which include minor SS contributions, agree with corresponding fits to experiment to within 10%. In transition metal complexes, however, the SOC contributions are generally much more dominant.[31] Accordingly, the fifth and sixth columns of Table 1 and Figure 2 compare the SOC contributions predicted by SCF-CI and our SDFT-PT implementation. These results show fairly good agreement between the former method, which is accurate but generally impractical for large metal complexes, and the latter. Thus, SDFT-PT predicts fairly accurately, as compared to both experiment and high level theory, for a set of diatomics whose ZFS differ over an order of magnitude ($D \approx +3\ cm^{-1} \leftrightarrow D \approx +20\ cm^{-1}$). Importantly, for the diatomics listed in Table 1, SDFT-PT predicts not only the magnitudes but also the positive signs of D, which, in general, can be positive or negative. Additional SDFT-PT calculations (to be published elsewhere) on a metal complex with known negative D produced the correct (negative) sign.[36] This further illustrates the fact that SDFT-PT can correctly predict the signs of the ZFS parameters.

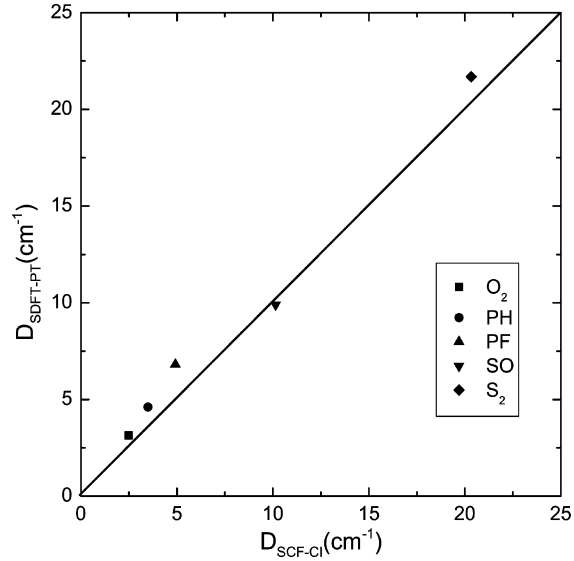

Figure 2. Comparison of SDFT-PT and SCF-CI[25] calculations of SOC contribution to axial ZFSs of selected diatomic molecules. Numerical values are given in Table 1.

3.2. Comparison with EPR Experiments: ZFS of Diatomic Sulfur. To illustrate the accuracy of SDFT-PT, we compare its results against those from EPR for a diatomic for which the SOC contribution to the ZFS is dominant. Wayne et al. recorded gas-phase EPR spectra on diatomic sulfur,[42] and analysis to their data yielded a rather large ZFS ($D_{SOC+SS}^{experiment} = +23.54\ cm^{-1}$), which includes a minor SS contribution ($D_{SS} \approx +0.26\ cm^{-1}$).[25]

The SDFT-PT values are in fairly good agreement with EPR. There is a small dependence on the exchange-correlation functional with U-BLYP[43,44] ($D^{SDFT-PT} = +21.69\ cm^{-1}$) predicting slightly greater values than those of U-BPW91[43,45] ($D^{SDFT-PT} = +19.82\ cm^{-1}$). Although our main motivation for implementing the SDFT-PT method was the treatment of transition metal complexes, the present results show that it can also be used for organic and other nonmetallic complexes when the SOC

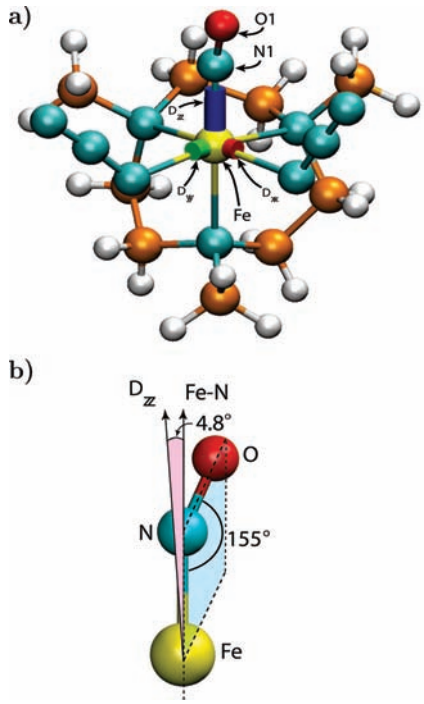

Figure 3. (a) S = 3/2 complex $FeL(NO)(N_3)_2$ showing orientations and relative magnitudes of principal components of the ZFS tensor with numerical values given in Table 2. (b) The largest component, D_{zz}, is in the Fe−N−O plane and rotated by only 4.8° with respect to the Fe−N(O) bond.

contribution to their ZFS is dominant. Systems that display sizable SS interactions, however, would require the additional calculation of the SS contribution to their ZFS.

3.3. ZFSs of an Iron Nitrosyl Complex. To interpret the large ZFS parameters of $\{FeNO\}^7$ (S = 3/2) complexes, we have performed SDFT-PT calculations on one such complex with the formula $FeL(NO)(N_3)_2$ (L = $C_9H_{21}N_3$).[46] The complex (Figure 3) was reported as the first crystallographically characterized octahedral $\{FeNO\}^7$ system with S = 3/2 ground state and has a tridentate macrocycle, which is facially coordinated. Debrunner et al.[47] performed 4.2 K Mössbauer measurements on the complex and determined parameters characteristic of $\{FeNO\}^7$ (S = 3/2) systems (i.e., $\delta_{Fe} = 0.62$ mm/s, and $\Delta E_Q = 1.31$ mm/s). The Mössbauer isomer shifts of $FeL(NO)(N_3)_2$ are intriguing, being smaller in magnitude than expected for high-spin ferrous and larger than expected for high-spin ferric configurations.[11] In addition, fits of spectroscopic data show that $\{FeNO\}^7$ (S = 3/2) complexes display unusually large ZFSs.[11−14] In particular, the value $D = 20 \pm 2$ has been reported for $FeL(NO)(N_3)_2$ from susceptibility measurements.[10] Therefore, it is clear that $\{FeNO\}^7$ (S = 3/2) complexes have an intricate valence electronic structure, which is ultimately responsible for their intriguing isomer shifts and large ZFSs. This is consistent with the works of Enemark and Feltham[1,2] that describe transition metal nitrosyls as highly covalent entities.

We have made a very accurate calculation of the ZFS parameters of $FeL(NO)(N_3)_2$. The computed ZFS parameters were fairly close for both functionals with U-BLYP yielding somewhat greater values than U-BPW91. As shown in Table 2, there is some dependence on the basis set with larger basis yielding somewhat larger values. The calculated D values for the two exchange-correlation functionals were in good agreement with experiment, all being within or close to the reported uncertainty of the susceptibility measurements. This

TABLE 2: Predicted and Experimental Values of ZFS Parameters of S = 3/2 Complex $FeL(NO)(N_3)_2$

	SDFT-PT		
	U-BLYP	U-BPW91	
	6-31G*/6-311G*	6-31G*/6-311G*	experiment[10]
D (cm^{-1})	+21.58/+25.04	+19.77/+22.87	+20, ±, 2
E, (cm^{-1})	+0.49/+0.55	+0.48/+0.54	NA[a]
(D_{xx}, D_{yy}, D_{zz})[b]	(−6.698, −7.687, +14.385)	(−6.110, −7.071, +13.181)	NA[c]

[a] No experimental value was reported for E, implying that it is small or close to zero. [b] Tensor components shown for 6-31G* basis. The 6-311G* basis displays similar trends. [c] D tensor components are not explicitly reported.

is consistent with our previous[29] SDFT-PT calculations on a different iron complex, which yielded excellent agreement with experiment.[29] Our calculations were also sensitive to a small, but finite, value of E. This is consistent with a small inequivalence of the orientation of the Fe−N−O plane with respect to the two azido ligands in the published crystallographic structure.

Equation 8 shows that computed ZFS parameters depend strongly on the energy denominators $\epsilon_{i\sigma} - \epsilon_{j\sigma'}$. For the two exchange-correlation functionals mentioned above, the SDFT-PT methodology yielded fairly accurate D values. We notice, however, that other functionals that incorporate an admixture of Hartree−Fock exchange[48] tend to give ZFS values, which are low in magnitude relative to experiment due to their tendency to produce $\epsilon_{i\sigma} - \epsilon_{j\sigma'}$ gaps, which are larger than those of pure exchange functionals.

3.4. Magneto-Structural-Experimental Correlations Obtained from SDFT-PT Methodology. Fits of magnetic susceptibility data or spectroscopic techniques, such as Mössbauer and EPR, do not normally allow for a rigorous mapping of the ZFS parameters to the molecular structure. By contrast, our SDFT-PT calculations have allowed us to map the magnitudes and orientations of the ZFS tensor to the molecular structure. Therefore, our results provide a much needed link between molecular structure, electronic structure, and spectroscopic parameters. As shown in Figure 3, the principal axis (*zz*), which is determined by the orientation of the largest tensor component D_{zz}, is in the Fe−N−O plane and very closely oriented along the Fe−N(O) bond. The figure shows that D_{zz} makes an angle of only 4.8° with respect to Fe−N(O). To rationalize this behavior, we briefly describe the composition of some relevant molecular orbitals (MOs) with respect to a coordinate system where iron is at the origin and the *z*-axis is defined by the Fe−N(O) bond.

The composition of the frontier MOs was extensively described in a previous study[11] and provides significant insight about the origin of the large axial ZFS parameter of $FeL(NO)(N_3)_2$. For convenience, we refer the two azido ligands as $(N_3)_A$ and $(N_3)_B$. As shown in Figure 4, occupied MO 87β is delocalized throughout the three fragments of the complex and has main contributions from NO, $(N_3)_A$, and Fe(3d) orbitals. The contour shows a strong π-bonding interaction between Fe(d_{xz}) and NO $\pi^*(p_x)$, which allows for substantial overlap between iron and ligand orbitals. The occupied MO 86β (not shown) is also delocalized throughout the molecule with main contributions from NO, $(N_3)_B$, and Fe(3d) orbitals. MO 86β displays a strong π-bonding interaction between Fe(d_{yz}) and NO $\pi^*(p_y)$, which also allows for strong overlap between iron and ligand orbitals. Thus, MOs 86β and 87β have very similar characteristics and are responsible for strong delocalization of

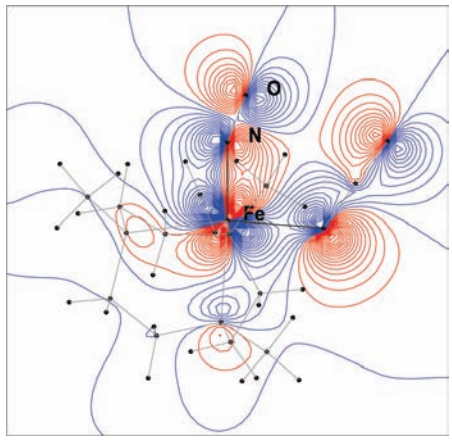

Figure 4. MO 87β of FeL(NO)$(N_3)_2$. The isovalue contour plot was obtained from SDFT calculations at the U-BPW91/6-311G* level. The plot is in the xz plane and shows the π-bonding interaction between Fe(d_{xz}) and NO $\pi^*(p_x)$ orbitals. The π-bond allows strong electron delocalization along the Fe−N(O) axis. This is consistent with the largest tensor component, D_{zz}, being very nearly oriented along the Fe−N(O) bond (Figure 2b). The contour also shows delocalization toward one of the N_3 ligands. MO 86β (not shown) has similar characteristics.[11]

two spin-down (β) electrons between NO(π^*) and two iron orbitals, Fe(d_{yz}) and Fe(d_{xz}), which are oriented along the z-axis. Such delocalization along the Fe−N(O) bond, which defines the z-axis, is fully consistent with the large magnitude and orientation of the largest component, D_{zz}, of the ZFS tensor (Figure 2b). The nearly coincident orientation of D_{zz} with the Fe−N(O) bond is also consistent with the very strong field character of the NO ligand according to its relative position in the spectrochemical and magnetochemical series.[49]

Plots of the partial density of states (DOS) provide further insight about the valence electronic structure and its relationship to the ZFS of the iron complex. Figure 5 shows that around the α-highest occupied molecular orbital (HOMO) energy region, the DOS has significant contributions from Fe(3d) and $(N_3)_{A,B}$ shells and, to a lesser extent, from NO(2p) and TACN N(2p). The DOS at the α-lowest unoccupied molecular orbital (LUMO) energy and higher is dominated by contributions from NO(2p) and, to a lesser extent, Fe(3d) shells. The DOS around the β-HOMO region has contributions from $(N_3)_{A,B}$, Fe(3d), and NO(2p) shells, whereas the β-LUMO region has a main contribution from Fe(3d) and, at higher energies, from NO(2p).

Figure 6 displays the energies of the frontier orbitals and shows that the α HOMO−LUMO gap (1.4 eV) is smaller than the corresponding β-gap (1.7 eV). The figure also shows how the smallest energy differences between occupied and unoccupied orbitals, $|\epsilon_i - \epsilon_j|$, arise from combinations of α-HOMOS and β-LUMOS. Equation 8 shows that small $|\epsilon_i - \epsilon_j|$ promote large ZFS. This is consistent with an analysis of the contributions to the axial ZFS splitting. Table 3 shows that the admixture of majority (α) occupied orbitals with minority (β) unoccupied orbitals produces the largest contribution to the ZFS. In fact, Table 3 also shows that the second largest contribution arises from admixtures of minority occupied orbitals with minority unoccupied orbitals. It is noteworthy that the two largest contributions involve minority LUMOs, which, as shown in the DOS plots, have substantial contribution fron NO(2p) orbitals underscoring the prominent role of the NO ligand on the large ZFS.

The DOS and composition of frontier orbitals show that FeL(NO)$(N_3)_2$ has a complex valence electronic structure.

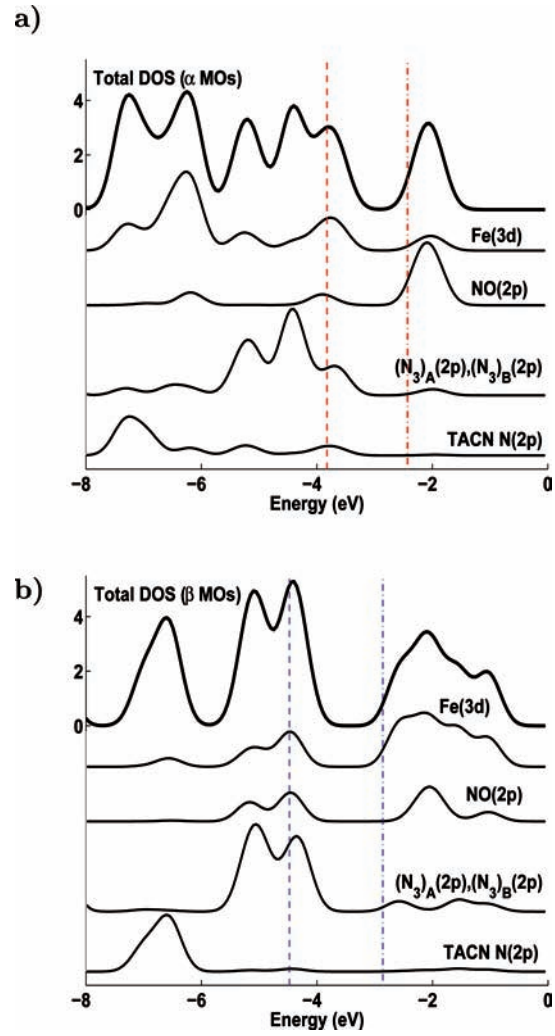

Figure 5. Total and partial DOS corresponding to (a) spin up (α) and (b) spin down (β) frontier orbitals of FeL(NO)$(N_3)_2$. The partial DOS were calculated for contributions from basis functions centered on the Fe(3d), NO(2p), $(N_3)_A$(2p), and $(N_3)_B$(2p) shells. In addition, partial DOS are also shown for the 2p shells of the three TACN nitrogens bound to iron. The left and right vertical lines correspond to the energies of the (α,β)-HOMO and (α,β)-LUMO, respectively. Orbital energies were obtained at the U-BPW91/6-31G* level.

However, despite the accuracy of magnetic susceptibility experiments[10] and extensive electronic structure calculations,[11] the relationship between the microscopic electronic structure and large ZFS of FeL(NO)$(N_3)_2$ had not been fully understood. The present analysis provides insight about the origin of the large ZFS and establishes a direct correlation between strong electron delocalization along the Fe−N(O) bond and the magnitude and orientation of the dominant tensor component D_{zz}. In addition, fitting of susceptibility data, by itself, did not allow for a rigorous mapping of the ZFS parameters to the molecular structure. By contrast, as shown in Figure 3, the magnitudes and orientations of the ZFS tensor obtained from our calculations have been plotted with respect to the molecular structure. Thus, the present SDFT-PT calculations provide important correlations between ZFS parameters and molecular structure, which are not normally obtained by standard fits to experimental data.

4. Conclusions

The results presented in this work give rise to the following conclusions.

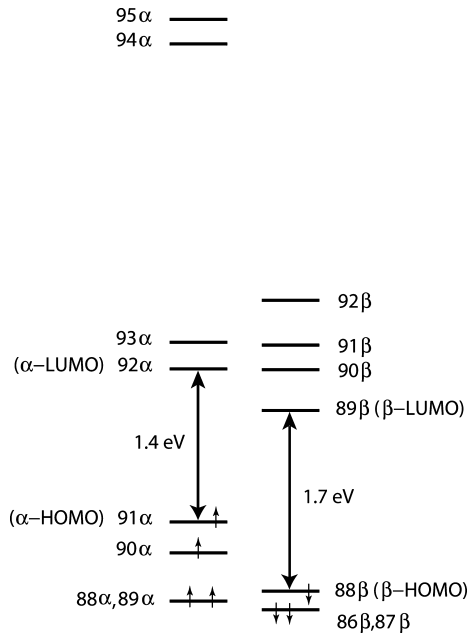

Figure 6. Energy level diagram of spin up (α) and spin down (β) frontier KS orbitals of $FeL(NO)(N_3)_2$.

TABLE 3: Partial Contribution to ZFS Parameters of $FeL(NO)(N_3)_2$ from Sets of Occupied and Unoccupied Orbitals[a]

occupied	unoccupied	(D, E) (cm^{-1})
majority	majority	(+3.44, +0.25)
majority	minority	(+13.83, +0.34)
minority	majority	(−1.47, −0.31)
minority	minority	(+4.07, +0.23)

[a] Orbitals obtained at the U-BPW91/6-31G* level.

(i) The SDFT-PT methodology allows, quite generally, the accurate computation of ZFSs of molecular systems that range from small diatomics to inorganic and bioinorganic complexes. Very importantly, the calculations yield not only the magnitude but also the sign of the ZFS parameters.

(ii) We have computed the ZFS parameters of $FeL(NO)(N_3)_2$ and have obtained fairly accurate values for this important complex. In addition, we have shown that the largest tensor component, D_{zz}, is very closely oriented along the Fe−N(O) bond, indicating that NO, a strong-field ligand, dominates the electronic structure of the complex.

(iii) Many fits of experimental data do not normally allow for a rigorous mapping of the ZFS parameters to the molecular structure. By contrast, our SDFT-PT calculations have allowed us to map the magnitudes and orientations of the ZFS tensor to the molecular structure. Therefore, our results provide a much needed link between molecular structure, electronic structure, and spectroscopic ZFS parameters.

(iv) The spin Hamiltonian (2) has been extensively used in the analysis of experimental data of bioinorganic complexes and metalloenzymes.[10,11,17,50] Thus, the present SDFT-PT method for predicting ZFS parameters has the potential to aid in the interpretation of a large amount of experimental data.

(v) The SDFT-PT methodology allows for a much broader range of applications. In particular, SDFT-PT calculations are useful for the computational design of complexes with large and "negative" ZFS for potential highly dense memory storage[26−28] applications.

Acknowledgment. This research was funded by NSF Career Award CHE-0349189 (J.H.R.). Computer time was provided by the National Center for Supercomputer Applications (NCSA) via Grant CHE-090020 (J.H.R.) and by Purdue University's ITaP Research Computing Center.

References and Notes

(1) Enemark, J. H.; Feltham, R. D. *Coord. Chem. Rev.* **1974**, *13*, 339.
(2) Enemark, J. H.; Feltham, R. D.; Huie, B. T.; Johnson, P. L.; Swedo, K. K. *J. Am. Chem. Soc.* **1977**, *99*, 3285.
(3) We follow Enemark[1] in representing an iron nitrosyl complex with seven valence electrons, Fe(3d) plus NO(π^*), as $\{FeNO\}^7$.
(4) Danon, J. *J. Chem. Phys.* **1963**, *39*, 236.
(5) Ballhausen, C. J.; Gray, H. B. *Inorg. Chem.* **1963**, *2*, 246.
(6) Manoharan, P. T.; Gray, H. B. *J. Am. Chem. Soc.* **1965**, *87*, 3340.
(7) Mingos, D. *Inorg. Chem.* **1973**, *12*, 1209.
(8) Wells, F. V.; McCann, S. W.; Wickman, H. H.; Kessel, S. L.; Hendrickson, D. N.; Feltham, R. D. *Inorg. Chem.* **1982**, *21*, 2306.
(9) Hodges, K.; Wollmann, R.; Kessel, S.; Hendrickson, D.; Derveer, D. V.; Barefield, E. K. *J. Am. Chem. Soc.* **1979**, *101*, 906.
(10) Brown, C. A.; Pavlosky, M. A.; Westre, T. E.; Zhang, Y.; Hedman, B.; Hodgson, K. O.; Solomon, E. I. *J. Am. Chem. Soc.* **1995**, *117*, 715.
(11) Rodriguez, J. H.; Xia, Y. M.; Debrunner, P. G. *J. Am. Chem. Soc.* **1999**, *121*, 7846.
(12) Arciero, D. M.; Lipscomb, J. D.; Huynh, B. H.; Kent, T. A.; Münk, E. *J. Biol. Chem.* **1983**, *258*, 4981.
(13) Orville, A. M.; Chen, V. J.; Kriauciunas, A.; Harpel, M. R.; Fox, B. G.; Münck, E.; Lipscomb, J. D. *Biochemistry* **1992**, *31*, 4602.
(14) Debrunner, P. G. *Hyperfine Interact.* **1990**, *53*, 21.
(15) Nocek, J. K.; Kurtz, D. M., Jr.; Sage, J. T.; Debrunner, P. G.; Maroney, M. J.; Que, L., Jr. *J. Am. Chem. Soc.* **1985**, *107*, 3382.
(16) Nocek, J. K.; Kurtz, D. M., Jr.; Sage, J. T.; Debrunner, P. G.; Shiemke, A. K.; Sanders-Loehr, J.; Loehr, T. M. *Biochemistry* **1988**, *27*, 1014.
(17) Kahn, O. *Molecular Magnetism*; VCH: New York, 1993.
(18) Kohn, W.; Sham, L. *J. Phys. Rev.* **1965**, *140*, A1133.
(19) Parr, R. G.; Yang, W. *Density-Functional Theory of Atoms and Molecules*; Clarendon Press: Oxford, 1989.
(20) Kohn, W.; Becke, A. D.; Parr, R. G. *J. Phys. Chem.* **1996**, *100*, 12974.
(21) Rodriguez, J. H.; Ok, H. N.; Xia, Y. M.; Debrunner, P. G.; Hinrichs, B. E.; Meyer, T.; Packard, N. *J. Phys. Chem.* **1996**, *100*, 6849.
(22) Rodriguez, J. H.; Xia, Y. M.; Debrunner, P. G.; Chaudhuri, P.; Wieghardt, K. *J. Am. Chem. Soc.* **1996**, *118*, 7542.
(23) Pederson, M. R.; Khanna, S. N. *Phys. Rev. B* **1999**, *60*, 9566.
(24) Pederson, M. R.; Kortus, J.; Khanna, S. N. *J. Appl. Phys* **2002**, *91*, 7149.
(25) Wayne, F. D.; Colbourn, E. A. *Mol. Phys.* **1977**, *34*, 1141–1155.
(26) Sessoli, R.; Gatteschi, G.; Caneschi, A.; Novack, M. A. *Nature* **1993**, *365*, 141.
(27) Wernsdorfer, W.; Allaga-Alcalde, N.; Hendrickson, D. N.; Christou, G. *Nature* **2002**, *416*, 406.
(28) Wang, S.; Zuo, J.; Zhou, H.; Choi, H.; Ke, Y.; Long, J. R.; You, X. *Angew. Chem., Int. Ed.* **2004**, *43*, 5940.
(29) Aquino, F.; Rodriguez, J. H. *J. Chem. Phys.* **2005**, *123*, 204902.
(30) Malkin, V. G.; Malkina, O. L.; Casida, M. E.; Salahub, D. R. *J. Am. Chem. Soc.* **1994**, *116*, 5898–5908.
(31) Weltner, W., Jr. *Magnetic Atoms and Molecules*; Dover: New York, 1989.
(32) Hehre, W. J.; Radom, L.; Schleyer, P. V.; Pople, J. A. *Ab Initio Molecular Orbital Theory*; John Wiley & Sons: New York, 1986.
(33) Rodriguez, J. H.; Wheeler, D. E.; McCusker, J. K. *J. Am. Chem. Soc.* **1998**, *120*, 12051.
(34) Rodriguez, J. H.; McCusker, J. K. *J. Chem. Phys.* **2002**, *116*, 6253.
(35) Casida, M. E.; Malkin, V. G.; Malkina, O. L.; Salahub, D. R. *J. Am. Chem. Soc.* **1994**, *116*, 5898.
(36) Aquino, F. Rodriguez, J. H. Unpublished results.
(37) Frisch, M. J.; Trucks, G. W.; Schlegel, H. B.; Scuseria, G. E.; Robb, M. A.; Cheeseman, J. R.; Zakrzewski, V. G.; Montgomery, J. A., Jr.; Stratmann, R. E.; Burant, J. C.; Dapprich, S.; Millam, J. M.; Daniels, A. D.; Kudin, K. N.; Strain, M. C.; Farkas, O.; Tomasi, J.; Barone, V.; Cossi, M.; Cammi, R.; Mennucci, B.; Pomelli, C.; Adamo, C.; Clifford, S.; Ochterski, J.; Petersson, G. A.; Ayala, P. Y.; Cui, Q.; Morokuma, K.; Malick, D. K.; Rabuck, A. D.; Raghavachari, K.; Foresman, J. B.; Cioslowski, J.; Ortiz, J. V.; Stefanov, B. B.; Liu, G.; Liashenko, A.; Piskorz, P.; Komaromi, I.; Gomperts, R.; Martin, R. L.; Fox, D. J.; Keith, T.; Al-Laham, M. A.; Peng, C. Y.; Nanayakkara, A.; Gonzalez, C.; Challacombe, M.; Gill, P. M. W.; Johnson, B.; Chen, W.; Wong, M. W.; Andres, J. L.; Gonzalez, C.; Head-Gordon, M.; Replogle, E. S.; Pople, J. A. *Gaussian 98*, Revision A.4; Gaussian, Inc.: Pittsburgh, PA, 1998.

(38) Welch, W. M.; Mitzushima, M. *Phys. Rev. A* **1972**, *5*, 2692–2695.
(39) Rostas, J.; Cossart, D.; Bastien, J. R. *Can. J. Phys.* **1974**, *52*, 1274–1287.
(40) Colin, R.; Devillers, J.; Prevot, F. *J. Mol. Spectrosc.* **1972**, *44*, 230–235.
(41) Davies, P. B.; Wayne, F. D.; Stone, A. *J. Mol. Phys.* **1974**, *28*, 1409–1422.
(42) Wayne, F. D.; Davies, P. B.; Thrush, B. A. *Mol. Phys.* **1974**, *28*, 989–996.
(43) Becke, A. D. *Phys. Rev. A* **1988**, *38*, 3098.
(44) Lee, C.; Yang, W.; Parr, R. G. *Phys. Rev. B* **1988**, *37*, 785.
(45) Perdew, J. P.; Wang, Y. *Phys. Rev. B* **1992**, *45*, 13244.
(46) Pohl, K.; Wieghardt, K.; Nuber, B.; Weiss, J. *J. Chem. Soc., Dalton Trans.* **1987**, 187–192.
(47) See footnote 4 of Nocek et al.[16]
(48) Becke, A. D. *J. Chem. Phys.* **1993**, *98*, 1372.
(49) Reed, C. A. *Inorg. Chim. Acta* **1997**, *263*, 95–97.
(50) Rohde, J.; In, J.; Lim, M. H.; Brennessel, W.; Bukowski, M.; Stubna, A.; Munck, E.; Nam, W.; Que, L., Jr. *Science* **2003**, *299*, 1037–1039.

JP8107667